Bacterial filamentation drives colony chirality

Andrés Aranda-Díaz[1], Cecilia Rodrigues[2,3], Alexandra Grote[1], Jiawei Sun[1], Carl Schreck[4], Oskar Hallatschek[4], Anton Souslov[5], Wolfram Möbius[2,3,†], Kerwyn Casey Huang[1,6,7,†]

[1]Department of Bioengineering, Stanford University, Stanford, CA, USA

[2]Living Systems Institute, University of Exeter, Exeter EX 4QD, United Kingdom

[3]Physics and Astronomy, College of Engineering, Mathematics and Physical Sciences, University of Exeter, Exeter EX4 4QL, United Kingdom

[4]Department of Physics, University of California at Berkeley, Berkeley, CA, USA

[5]Department of Physics, University of Bath, Bath BA2 7AY, United Kingdom

[6]Department of Microbiology and Immunology, Stanford University School of Medicine, Stanford, CA 94305, USA

[7]Chan Zuckerberg Biohub, San Francisco, CA 94158

[†]Corresponding authors: kchuang@stanford.edu and w.moebius@exeter.ac.uk

Running title: *Filamentation drives colony chirality*

Keywords: A22, MreB, cephalexin, cell division, anaerobic growth, temperature, peptidoglycan, cell wall

Abstract

Chirality is ubiquitous in nature, with consequences at the cellular and tissue scales. As *Escherichia coli* colonies expand radially, an orthogonal component of growth creates a pinwheel-like pattern that can be revealed by fluorescent markers. To elucidate the mechanistic basis of this colony chirality, we investigated its link to left-handed, single-cell twisting during *E. coli* elongation. While chemical and genetic manipulation of cell width altered single-cell twisting handedness, colonies ceased to be chiral rather than switching handedness, and anaerobic growth altered colony chirality without affecting single-cell twisting. Chiral angle increased with increasing temperature even when growth rate decreased. Unifying these findings, we discovered that colony chirality was associated with the propensity for cell filamentation. Inhibition of cell division accentuated chirality under aerobic growth and generated chirality under anaerobic growth. Thus, regulation of cell division is intrinsically coupled to colony chirality, providing a mechanism for tuning macroscale spatial patterning.

Introduction

An object is chiral if it is distinguishable from its mirror image. Chirality is prevalent throughout nature at all scales, and stereoisomers are often functionally distinct, from our left and right hands to L- and D-amino acids that are used for metabolism/translation and bacterial cell-wall synthesis, respectively. Chirality is manifest in polymers that form helices, such as bacterial flagella and cytoskeletal filaments (1, 2). Chirality can also be an intrinsic property of individual cells; for instance, myosin in *Drosophila* can reverse handedness in cells, which feeds forward to affect organ handedness (3). Chirality drives the development of left-right asymmetry generation in organs of *Drosophila melanogaster* (4) and in the *Caenorhabditis elegans* embryo (5). Plants twist as they grow, and mutants in SPIRAL2 change that twist from left- to right-handed; this handedness reversal is coupled to a switch from anisotropic growth to isotropic growth (6). However, it is largely unknown how chirality at the tissue and organismal scales is linked to cellular and molecular properties. Here, we investigate the link between chirality and growth at the micron scale of individual bacterial cells and chirality at the millimeter scale of colonies, visible to the naked eye.

Many rod-shaped bacterial cells exhibit twisting at the single-cell level during growth. In the Gram-negative bacterium *Escherichia coli*, growth occurs along the body of the cell and not at the poles (7). As the two ends move apart from one another, they also rotate in opposite directions, representing left-handed twist (Fig. 1A) (8). Twisting has also been observed in the Gram-positive *Bacillus subtilis* (9), in a right-handed manner (8). Bacterial growth requires expansion of the cell wall, a rigid macromolecule composed of crosslinked

glycan strands (10) that is necessary and sufficient for cell-shape determination (11). A biophysical model of cell-wall growth quantitatively predicted the degree of cell twisting generated by a helical pattern of insertion, which produced cell-wall material with the opposite handedness (8, 12). The bacterial actin homolog MreB (13), which is responsible for the spatiotemporal patterning of cell wall material (7), was required for cell twisting (8). The small molecule A22 depolymerizes MreB; at high concentrations, cells eventually round up and lyse (14). Twisting of *E. coli* cells is tunable: as cells widen under increasing sublethal levels of A22 treatment (15), the angle of MreB motion, which is thought to signify the placement of new strands of cell wall material (16), rotates and ultimately adopts an angle on the opposite side of the line perpendicular to the long axis of the cell, signifying a gradual conversion of twisting from left- to right-handed (15).

Bacterial colonies can also exhibit chirality during growth (17-19). This effect is striking in experiments investigating range expansions, in which otherwise genotypically and phenotypically identical cells producing fluorescent proteins of two different colors (purely for the purposes of distinguishing genotypes) are inoculated onto an agar plate to grow into a colony. As the colony expands, cells on the exterior have preferential access to uncolonized surface area and nutrients, leading to spatial segregation of the two fluorophores in well-defined “sectors” that expand outward, ultimately producing a pinwheel pattern. Boundaries between these sectors provide a frozen record of colony growth that displays a chiral angle (19). On top of the wiggling motion of boundaries between sectors, the boundaries of many species such as *E. coli* exhibit deterministic chirality in the form of expansion biased along the edge of the colony (17). Ultimately, cells

80 themselves are likely to generate the observed behavior at the colony scale, although
81 colony chirality must also be dependent on environmental conditions such as adhesion and
82 surface wetness, both of which dictate cell motility. Indeed, *E. coli* colony chirality was
83 shown to be mediated by close interactions between cells and the surface, with expression
84 of pili and other adhesive structures suppressing chirality, and agar stiffness affecting
85 chirality (20). There are also strain-specific differences in colony chirality (20), even
86 though twisting at the single-cell level is relatively constant (8). Previous studies that
87 attempted to explore the relationship between cell shape or cell-wall synthesis and colony
88 chirality made comparisons between different species (20). However, a systematic
89 interrogation of the links between single-cell properties and colony chirality through
90 environmental, genetic, and physiological perturbations has not been undertaken. In
91 particular, it is critical to employ a strategy that tunes behaviors such as twisting in a single
92 organism in order to probe potential couplings with colony chirality.
93
94 Here, we set out to determine the relationship between cell shape, twisting and
95 handedness at the single-cell level, and macroscopic colony chirality. Using single-cell and
96 colony imaging, we found that A22 treatment and anaerobic growth inhibited growth and
97 reduced colony chirality to near zero, making it unclear whether single-cell twisting was
98 responsible for the change in chiral angle. Cells at the edge of the colony adapted to A22
99 treatment by reducing their width and length. Chiral angle increased with increasing
100 temperature, even at high temperatures that caused a decrease in growth, indicating that
101 growth rate does not determine colony chirality. Across all conditions, the presence of
102 chiral colonies was associated with filamentous cells at the edge of the colony, and

103 antibiotic inhibition of division resulted in enhanced chirality. These results reveal a
104 complex connection between single-cell dimensions and population level spatial patterns,
105 underscoring the role of cell division in determining colony chirality.

Results

E. coli DH5α cells exhibit similar single-cell twisting as MG1655

Chirality in *E. coli* colonies is readily observed when using strain DH5α (17, 19), with a clockwise rotation when viewed from the top. A recent comparison between *E. coli* strains revealed that on low-salt LB agar, *E. coli* MG1655 colonies also rotate clockwise, but exhibit less pronounced chirality than DH5α colonies (20). To determine whether this difference in chirality could be due to differences in twisting at the single-cell level (Fig. 1A), we utilized our previously developed Twist-n-TIRF method (15). In this method, cells are treated with the beta-lactam antibiotic cephalexin to block cell division, allowing for easier visualization of twisting. The cell wall is labeled uniformly with a stationary dye (in this case, Wheat Germ Agglutinin (WGA) labeled with Alexa Fluor 488 (7)), and then the bottom of the cell is bleached by a TIRF laser. As the cell subsequently grows, twisting causes bright, unbleached regions to rotate into the TIRF imaging plane (Fig. 1B), and the handedness and degree of twisting can be computed from the direction and rate of fluorescence appearance, respectively (15). Virtually all DH5α cells clearly twisted in a left-handed manner on LB agarose pads (Fig. 1C), similar to MG1655 on EZ-RDM pads (15) and consistent with our previous study employing beads bound to the outer membrane (8). Thus, left-handed twisting is conserved across *E. coli* strains and growth media.

Given the central role of MreB in single-cell twisting (8, 15), we next sought to quantify the effects of A22 treatment on DH5α. We treated log-phase DH5α cells expressing YFP or CFP from a plasmid for 3 h with a range of A22 concentrations from below to above the minimum

129 inhibitory concentration (~1 μg/mL) in LB (Methods). At higher A22 concentrations, Twist-
130 n-TIRF measurements revealed an increasing fraction of DH5α cells that exhibited right-
131 handed or ambiguous twisting (Fig. 1C), similar to the handedness reversal of MG1655 (15).
132 Cell shape also changed as expected from previous experiments with MG1655 (15): DH5α
133 cells increased in width and decreased in length as A22 concentration was increased (Fig.
134 1D). Thus, DH5α exhibits similar changes in twisting and cell shape across A22
135 concentrations as MG1655.
136
137 **A22 treatment reduces colony chirality**
138 The inversion of twisting handedness due to A22 treatment provides a qualitative change in
139 cellular behavior through which to interrogate the connection between single-cell and
140 colony-level behaviors. If single-cell twisting is the determinant of colony chirality, we
141 should see a change from clockwise to counter-clockwise rotation within colonies as single-
142 cell twisting changes with increasing A22 concentration. To test this hypothesis, we grew
143 mixed colonies of YFP- and CFP-expressing DH5α on LB plates at 37 °C with a range of A22
144 concentrations and imaged the colonies after 7 days of growth. As expected, the frozen
145 record revealed that colonies quickly developed into sectors of single colors (Fig. 2A). We
146 segmented the images, identified sector boundaries, plotted the change in angle against a
147 function of colony radius, and computed the chiral angle (Fig. 2A, Methods). In the absence
148 of A22, the chiral angle was θ=6.4° (Fig. 2B,C), similar to previous measurements (17, 20).
149 A22 treatment reduced the chiral angle to approximately zero (Fig. 2B,C), but even at high
150 concentrations there was not clear evidence for reversal of handedness, in seeming
151 contradiction to our hypothesis.

In a recent study, we showed that *E. coli* adapts to the cell widening effects of A22 treatment by increasing expression of *mreB*, resulting in a subsequent decrease in cell width (21). If adaptation that altered cellular dimensions occurred during colony growth, such changes could have confounded our above test of the effect of A22 and single-cell twisting on colony chirality. To test whether cells on LB plates with A22 changed morphology over time, we sampled cells from the edge of colonies once per day and imaged the cells to quantify their dimensions (Methods). As we suspected, cell width decreased steadily over the course of a week, reaching a relatively constant width displayed by cells on plates without A22 (Fig. 2D); coincident with the width decrease, length gradually increased (Fig. 2D). For the widest cells (~1.4 μm), the cell width measured on day 1 on LB+1.5 μg/mL A22 was equivalent to the cell width in liquid LB+0.5 μg/mL A22 (Fig. 1D). Under this condition, ~60% of cells exhibited no or ambiguous twisting (Fig. 1C), consistent with the lack of chirality at the colony level. Thus, adaptation of cell shape on plates prevents a direct test of whether A22-mediated reversal of single-cell twisting handedness necessarily reverses colony-chirality handedness.

Heterologous expression of a foreign cell-wall synthesis enzyme reverses single-cell twisting but colonies do not exhibit chirality

To circumvent adaptation associated with A22 treatment, we sought an alternate mechanism for altering cell width and single-cell twisting. We previously showed that heterologous expression of *mrdA*, which encodes the essential transpeptidase PBP2 (22), from *Vibrio cholerae* caused *E. coli* MG1655 cells lacking the endogenous *mrdA* gene to widen

and to reverse twisting handedness similar to A22 treatment (15). We constructed DH5α Δ*mrdA* strains with constitutive expression of *V. cholerae mrdA* (Vc-*mrdA*) and a plasmid coding for CFP or YFP from a parental strain DH5α-E, resulting in DH5α-E Δ*mrdA* Vc-*mrdA* CFP and DH5α-E Δ*mrdA* Vc-*mrdA* YFP (Methods). The mean cell width of these strains was significantly larger than DH5α-E or the DH5α-H strain used in the experiments above (Fig. 3A,B). DH5α-E Δ*mrdA* Vc-*mrdA* cells were highly sensitive to cephalexin, resulting in rapid lysis during Twist-n-TIRF experiments that precluded measurement of single-cell twisting. Unlike A22-treated wild-type cells, untreated fluorescent DH5α-E Δ*mrdA* Vc-*mrdA* cells remained wider and shorter than wild-type cells over 5 days of growth in colonies (Fig. S2). Colonies displayed highly reduced chiral angle (Fig. 3C,D), leaving it unclear whether reversal of handedness at the single-cell level results in reversed handedness of colony chirality.

Quenching of colony chirality between two surfaces is likely due to lack of twisting in anaerobic environments

We hypothesized that colonies sandwiched between two agar surfaces should not exhibit any chirality based on symmetry considerations, independent of changes in cell shape. To test this hypothesis, we inoculated a droplet of CFP-expressing and YFP-expressing DH5α cells as before, allowed the droplet to dry, and then placed another large agar pad on top of the agar plate (Fig. 4A). The colony continued to expand between these two surfaces, presumably due to the lack of agar crosslinking between the two pads as compared to within the pads. Cells emitted very little fluorescence, which we surmised was due to their lack of oxygen; anaerobic conditions prevent maturation of fluorescent proteins (23). GFP matures

198 more readily at low temperatures (24), hence we incubated sandwiched colonies at 4 °C
199 (Methods) and then quantified the fluorescence patterns. The sector boundaries were
200 essentially achiral (Fig. 4A,B, S3).
201
202 To test whether the absence of chirality was due to the restoration of symmetry at the
203 interface or to the depletion of oxygen, we grew a mixed colony on a single agar surface in
204 anaerobic conditions. We observed little to no chirality (Fig. 4C,D), indicating that anaerobic
205 growth is sufficient to abolish colony chirality. Colonies were smaller after 7 days of
206 anaerobic growth compared with aerobic growth. To test whether anaerobic growth
207 abolished single-cell twisting, we performed Twist-n-TIRF in anaerobic conditions
208 (Methods). Cells continued to twist in a left-handed fashion (Fig. 4E), thus lack of colony
209 chirality in anaerobic conditions is not due to lack of single-cell twisting. Instead, these
210 findings suggest that another, oxygen-dependent factor influenced the level of colony
211 chirality.
212
213 **Temperature alters growth rate and chirality without changing cell twisting**
214 After 7 days, colonies grown on LB+A22 (Fig. 2A) or anaerobically (Fig. 4C) were significantly
215 smaller than when grown aerobically on LB alone (Fig. 2A, 4C). Thus, we sought to test
216 whether growth rate was a major determinant of colony chirality. Temperature is well
217 known to modulate growth rate (25). In liquid, the maximum growth rate of DH5α increased
218 as a function of temperature up to an optimal temperature of ~42 °C (Fig. 5A, S4). We grew
219 mixed colonies across a range of temperatures and imaged them after 7 days (Fig. 5B).
220 Colony size was also temperature-dependent, with smaller colonies at 30 and 42 °C than at

37 °C (Fig. 5A). However, chiral angle increased monotonically with temperature up to 42 °C (Fig. 5C), indicating that chirality is regulated by a factor other than growth rate that changes with temperature.

Filamentation is linked to the extent of colony chirality

Single-cell twisting was approximately constant across temperatures (Fig. S5), again highlighting that another factor must be dictating chirality. Motivated by our observations that A22 treatment reduced cell length (Fig. 1D) and chiral angle (Fig. 2C), we measured log-phase DH5α cellular dimensions in liquid culture at various temperatures. Length and width both increased monotonically with temperature (26), with cells at 44 °C more than twice as long as those at 21 °C (Fig. S6). To verify whether cells were similarly elongated in colonies *in situ*, we imaged colonies directly and identified filamentous cells at the extreme edge of colonies with pronounced chirality (37 °C and 42 °C) (Fig. 6A), while less filamentation was apparent in colonies with little chirality (lower temperatures and anerobic growth) (Fig. 6 S7). Because of the difficulty in segmenting individual cells from *in situ* images of the colony, we sampled and imaged cells from the colony edge. We surmised that higher cell density in images was indicative of more sampling towards the center of the colony. Thus, to correct for variability in sampling location we focused our analysis on sets of images with similar cell density (Fig. S8). As in liquid, mean cell length increased with temperature and colonies grown at higher temperatures displayed more filamentous cells (Fig. 6B). Interestingly, cells grown in liquid had similar cellular dimensions aerobically and anaerobically, but cells sampled from the edge of colonies grown anaerobically were significantly shorter and wider

than those from the edge of aerobic colonies (Fig. 6C, S9). These observations are consistent with the hypothesis that some degree of cell filamentation is necessary for colony chirality.

Inhibition of cell division enhances chirality

To determine whether filamentation and chirality are causally linked, we sought to increase the fraction of filamentous cells within a colony. We grew mixed cultures at 37 °C on various concentrations of cephalexin, a beta-lactam antibiotic that inhibits the division-specific transpeptidase PBP3 (27). At higher concentrations, colonies exhibited pronounced chirality similar to 42 °C, and chiral angle increased in a dose-dependent manner (Fig. 7A, S10). To test whether cephalexin would introduce chirality in situations where the chiral angle was close to zero, we grew mixed cultures anaerobically on LB+10 μg/mL cephalexin plates. Remarkably, cephalexin-treated colonies exhibited obvious chirality (Fig. 7C). Thus, inducing filamentation is sufficient to introduce or accentuate colony chirality.

Discussion

In this study, we systematically measured the degree and handedness of twisting at the single-cell level across many perturbations, and determined that while changes that perturb single-cell twisting alter colony chirality, changes that perturb colony chirality do not necessarily alter single-cell twisting. It is clear that many factors interact to determine colony structure, including forces between cells and accessibility of nutrients (28), cellular geometry (29), and interactions of cells with each other and with the surface (20). Previous findings connecting surface attachment with colony chirality (20) are not inconsistent with our study, since the dependence of agar properties and surface attachment on temperature, cell size, and oxygen are unknown. Our colony chirality observations are phenomena that are either intrinsically three-dimensional or originate from cells being subject to a solid surface on one side and an air surface on the other, as confining the cells between two agar pads may eliminate chirality by removing the air-agar asymmetry (Fig. 4A). Regardless, our data highlight the role of cell filamentation in establishing colony chirality, with division-inhibiting cephalexin treatment leading to the introduction of chirality in colonies grown anaerobically (Fig. 7). Moreover, cell length is the variable that unifies colony chirality across all of our growth conditions. These results reveal a complex connection between single-cell dimensions and population level spatial patterns (30, 31).

Our original motivation for this study was to establish whether colony chirality can be traced back to single-cell behaviors. While we have shown that cell filamentation is coupled to the generation of colony chirality, it remains unclear whether single-cell twisting is also a factor. A22 treatment does reduce chirality (Fig. 2) as does genetic manipulation of the cell-wall

279 synthesis machinery (Fig. 3). Moreover, single-cell twisting and colony chirality each have a
280 defined handedness in the absence of A22. However, it remains unclear whether and how
281 handedness at the microscopic scale determines handedness at the macroscopic scales.
282
283 The connection between filamentation, and more generally cell shape, and colony
284 patterning was unexpected, in part because the regulation of division across environmental
285 conditions such as A22 treatment, anaerobic growth, and temperature are poorly
286 understood. In the case of A22, it was critical to measure cell shape at the edge of the
287 colony, which revealed that the cell width phenotype characteristic of A22 treatment on
288 short time scales was reversed after several days (Fig. 2D), likely due to transcriptional
289 adaptation (21). It is intriguing that regulation of cell division takes place on such long time
290 scales. The tunability of chirality using cephalexin provides an interesting control knob for
291 the design of macroscale patterns in bacterial communities.
292
293 What are the origins of colony chirality? Ultimately, chirality must materialize from some
294 molecular symmetry breaking, and while the cell wall is an enticing candidate, the
295 extracellular environment cannot be ruled out. This knowledge gap motivates the
296 quantification of single-cell twisting and colony chirality across more strains and species, to
297 determine whether the two are generally coupled. An ideal demonstration would be the
298 reversal of handedness of a single species, as we attempted in this work, although it may be
299 impossible to construct a right-handed *E. coli* cell that is stable during filamentation without
300 reprogramming many cell-wall synthesis components.
301

A wealth of exotic patterns and mechanical properties can emerge from chiral constituents exerting forces on each other and their environments (32-34), including periodic crystals of rotating particles (35-37) that can synchronize into exotic phases (38). Mixtures of oppositely rotating particles tend to phase separate (39, 40), leading to complex structures and flows at chiral-phase interfaces (41, 42). Analyzing flow patterns and excitations of chiral active fluids has led to the design of topological states of matter (43, 44) and predictions of novel hydrodynamic responses (45, 46) that have been experimentally measured (47). Biological settings such as colony chirality may provide even more complex ways to connect microscopic forces of chiral active components to macroscopic handedness. For example, the observation that filamentation in only a few percent of cells is sufficient to induce chirality in anaerobically grown colonies motivates the study of mixtures of active particle with a heterogeneous distribution of geometries.

From an ecological and evolutionary perspective, what is the relevance of colony chirality? Recent work has suggested that chirality is an important population-level trait that mediates competition, invasion, and ultimately spatial structure within a bacterial community (48). If so, then our work suggests that colony-scale patterning has likely applied selective pressures on division at the cellular-scale. To design the spatial structure of bacterial communities, it is advantageous to control the emergent pattern of cell growth rather than have to establish patterns from the start. To achieve this control will ultimately require a mechanistic model for colony chirality, the development of which will be facilitated by the discovery that cellular properties such as cell length are critical parameters.

Materials and Methods

Bacterial strains and plasmids

Strains used in this study are described in Table S1. In brief, we used three pairs of strains. In each pair, the two strains have a common genetic background and carry plasmids expressing CFP or venus YFP. The pair used for the majority of experiments is identical to the one used in previous studies reporting colony chirality (17, 19, 20). In each pair, there were no obvious fitness differences between the two strains (both strains were able to form sectors). Fluorescence levels were sufficient for imaging even for basal expression in the absence of IPTG, hence we did not include IPTG in any of the media.

For this study, we constructed *E. coli* DH5α Δ*mrdA* strains with constitutive expression of *V. cholerae mrdA* by replacing the genomic *E. coli mrdA* sequence with a 4169-bp PCR fragment encoding the *V. cholerae mrdA* (Vc-*mrdA*) sequence and kanamycin resistance cassette, followed by selection for stability. Construction of the DH5α Δ*mrdA* strain was as follows: the Vc-*mrdA* DNA fragment was amplified from the pww308-VcmrdA construct (15) with primers that have 20 nucleotides of homology to the plasmid DNA sequence and 50 nucleotides of homology to the genomic Ec-*mrdA* target sequence, specifically delmrdAFor (5'-ACGCAGCGGATGAAACTACAGAACTCTTTTCGCGACTATACGGCAGAGCCACGTTGTGTCTCAAAATC-3') and delmrdARev (5'-TATCCGTCATGATTAATGGTCCTCCGCTGCGGCAACCGCTGGATTTTCCGCATCCTAGGTCATGGCTGTATTAC). The DH5α strain lacks the ability for homologous recombination. Therefore,

348 *E.coli* strain DH5α (Invitrogen) was first transformed with the pSIM5 plasmid (pSC101
349 repA^{ts}) encoding Red recombination proteins. Selection of transformed cells was
350 performed by growing in Lennox LB in the presence of 17.5 μg/mL chloramphenicol at 30
351 °C to allow pSIM5 replication, producing strain eCR106 that was able to perform
352 homologous recombination. eCR106 cells were transformed with the gel-purified Vc-*mrdA*
353 DNA fragment via electroporation as follows: eCR106 cells were grown at 30 °C to OD=0.4-
354 0.5, transferred to 42 °C for 15 min for induction of Red proteins, and then transferred to
355 ice for 10 min. Cells were centrifuged at 3000*g* and the pellet was washed with ice-cold
356 water twice before resuspending in 10% glycerol solution for electroporation using a
357 GenePulser XCell (BioRad) electroporator with the pre-set bacterial protocol for *E. coli*
358 using a 1-mm cuvette. After transformation, cells were incubated at 30 °C for 2 h before
359 selection on Lennox LB agar plates with 25 μg/mL kanamycin. Transformed cells were
360 identified by colony PCR with primers delBFor (5'–ACATCATCGCCTTAGACGTTC-3') and
361 delBRev (5'-AGATGGACTTTATCCCAGAATG-3') for the upstream/downstream *E. coli mrdA*
362 sequence and primers delCFor (5'-AGCGGATGAAACTACAGAACTC-3') and delCRev (5'-
363 CGGCAACCGCTGGATTTTC).
364
365 Colonies were picked and grown in Lennox LB at 37 °C to remove the pSIM5 plasmid,
366 creating strain eCR111. pSIM5 loss was confirmed by the absence of growth under
367 chloramphenicol selection. Genomic eCR111 DNA was extracted using a GeneJET Genomic
368 DNA Purification Kit (ThermoFisher) and used as DNA template for amplification with
369 primers delBFor and delCRev. The PCR fragment was sequenced using a MinION (Oxford

Nanopore Technologies). Sequencing results showed that the Tet promoter region of the Vc-*mrdA* fragment used for the recombination was lost in this strain.

CFP/YFP plasmids were constructed by cloning the fluorescent protein coding sequence into pSTV28 (Takara Bio Europe SAS) with EcoRI/SalI restriction sites. eCR111 cells were transformed with CFP/YFP constructs via electroporation as above, generating strains eCR112_1 with CFP and eCR112_2 with YFP. Selection of transformants was achieved using 35 µg/mL chloramphenicol.

Growth of mixed colonies

A step-by-step protocol is available online on protocols.io (https://www.protocols.io/view/growth-of-mixed-e-coli-colonies-bqgjmtun). In short, agar plates (6 cm in diameter) were prepared with 10 mL of Lennox LB (RPI, Cat. #L24066; Melford, Cat. #L24060-100.0 for colonies sandwiched between agar slabs and corresponding control experiments) with 1.5% agar (BD, Cat. #214530) and left on the bench overnight. Plates were used the next day or stored at 4 °C. As necessary, A22 or cephalexin were added from frozen stocks to the liquid after autoclaving. To initiate colony growth, the appropriate pair of fluorescent *E. coli* strains were grown overnight at 37 °C in liquid Lennox LB. Both cultures were diluted 10-fold in fresh LB and mixed. One microliter droplets were pipetted onto prewarmed plates and grown at 37 °C, typically for 7 to 8 days. Anaerobic growth experiments were carried out in a custom anaerobic chamber (Coy Lab Products). Colony growth between agar surfaces was achieved by cutting an agar pad out of a fresh plate and placing it upside down onto freshly inoculated cultures.

393

394 ***Sampling from mixed colonies***

395 Cells were sampled from the border of colonies using a 20-µL LTS micropipette tip
396 (Rainin). After touching the edge of the colony, cells were resuspended in 20 µL PBS and 1
397 µL was spotted onto PBS 1% agarose pads for imaging.

398

399 ***Imaging of mixed colonies***

400 Fluorescence images of colonies were acquired after 7-8 days of growth using a 1X
401 objective on a Nikon Eclipse Ti-E inverted fluorescence microscope equipped with a DU897
402 electron multiplying charged couple device (EMCCD) camera (Andor) using µManager v.
403 1.4 (49), or a Nikon TE-2000 or Zeiss Axio Zoom.V16 microscope. Colonies sandwiched
404 between two agar surfaces and the colonies in the corresponding control experiments were
405 imaged after 7 days at 4 °C. Colonies that did not show sufficient fluorescence at this point,
406 were imaged again after 26 more days at 4 °C.

407

408 Edges of colonies were imaged with a 20X objective on a Nikon Eclipse Ti-E inverted
409 fluorescence microscope equipped with a DU897 camera (Andor) using µManager v. 1.4.

410

411 ***Identifying colony radius and sector boundaries in mixed colonies***

412 Images were imported into Matlab. The difference between YFP and CFP images was used
413 to identify boundaries of intensity using the 'edge' function with the 'Log' method. The
414 center of the colony was defined by fitting a circle to 20 points manually selected from the
415 images either from the border of the colony if the colonies were small enough to fit in the

image, or from the border of the mixed-fluroescence sector at the center of the colony. The coordinates of the boundaries were transformed to polar coordinates based on the center of the colony. Points were mapped to traces by connecting nearest neighbors. Points too close to the center of the colony were discarded. Boundary traces were cleaned up manually: some were separated at a manually selected location when the traces clearly represented two sides of a sector, and some were removed because they clearly captured a feature that was not a sector boundary. Traces in polar coordinates were then smoothed. Some parameters (closeness to the center or the threshold for edge detected) were modified depending on the quality of the image. All traces from all colonies of a given experiment were then pooled. The mean was obtained by bootstrapping: random traces (selected with replacement) were averaged to calculate the slope, and then the slope was integrated to obtain a mean trace. This process was repeated 200 times to compute the final mean trace and the standard deviation over the 200 iterations.

All code is available in a GitHub repository https://github.com/aarandad/ColonyChirality-KCH.

Growth measurements in liquid culture

Optical density (OD) measurements were performed with an Epoch 2 plate reader (BioTek) at 37 °C with continuous shaking and OD_{600} measured at 7.5-min intervals. Maximal growth rate was calculated as the maximal slope of ln(OD) with respect to time (calculated from a linear regression of a sliding window of 11 timepoints) using custom Matlab R2018b (Mathworks) code.

Single-cell imaging

Cultures were grown overnight at 37 °C in LB, and diluted 1:200 into fresh medium (with antibiotics when appropriate). For phase-contrast imaging, cells were spotted onto a 1% (w/v) agarose pad with LB. Cells treated with A22 were exposed to the drug for 2-3 h before imaging.

Phase-contrast and epifluorescence images were acquired with a Nikon Ti-E inverted microscope (Nikon Instruments) using a 100X (NA 1.40) oil immersion objective and a Neo 5.5 sCMOS camera or a DU885 EMCCD (Andor Technology). The microscope was outfitted with an active-control environmental chamber for temperature regulation (HaisonTech, Taipei, Taiwan). Images were acquired using μManager v. 1.4 (49). Cell contours were automatically segmented using *Morphometrics* (50) and a local coordinate system was defined based on the meshing algorithm from *MicrobeTracker* (51). Some images of cells sampled from the edge of colonies (Fig. 6) had clusters of cells that could not be segmented by *Morphometrics*. These images were processed with the neural network-based machine learning framework *DeepCell* (52) prior to segmentation with *Morphometrics*.

Twist 'n' TIRF measurements

Fluorescent WGA was added to liquid cultures to a final concentration of 25 μg/mL. After 2.5 h of growth, cells were pelleted at 8,000*g* for 1 min and washed with PBS once before being spotted onto a 1% (w/v) EZ-RDM 0.2% glucose or LB agarose pads with 10 μg/mL cephalexin. For anaerobic Twist 'n' TIRF experiments, cultures were grown, washed, and

462 spotted onto agarose pads inside an anaerobic chamber. Mounted pads were fully sealed
463 with VALAP before removal from the anaerobic chamber and imaging was conducted
464 immediately.
465
466 ***TIRF microscopy***
467 Twisting measurements were performed on a Ti-E inverted microscope (Nikon, NY, USA)
468 with a 100X objective (NA 1.40). A Sapphire OPSL 488-nm laser (Coherent, CA, USA) was
469 coupled into a TIRF illuminator (Nikon) attached to the microscope stand. Images were
470 acquired with DU885 EMCCD (Andor, CT, USA) camera and synchronization between
471 components was achieved using μManager (49).
472
473 ***Cell twisting analysis***
474 In Twist 'n' TIRF experiments, cell contours were computationally extracted from phase
475 using Morphometrics (50). The integrated WGA fluorescence enclosed within the cell
476 contour was quantified. These values were normalized to the pre-bleached level and
477 plotted as a function of the change in length Δl relative to the pre-bleached length. Curves
478 were then fitted to extract the slope λ representing the rate of fluorescence recovery due to
479 twisting. The curves were fit over the first 3 μm of elongation to avoid noise from
480 photobleaching after large amounts of exposure.

Acknowledgements

We thank members of the Huang and Hallastchek lab for helpful discussions. This work was funded by NIH CAREER Award MCB-1149328 (to K.C.H.), the Allen Discovery Center at Stanford University on Systems Modeling of Infection (to K.C.H.). A.A.-D. is a Howard Hughes Medical Institute International Student Research fellow, a Stanford Bio-X Bowes fellow, and a Siebel Scholar. K.C.H. is a Chan Zuckerberg Investigator.

Figures

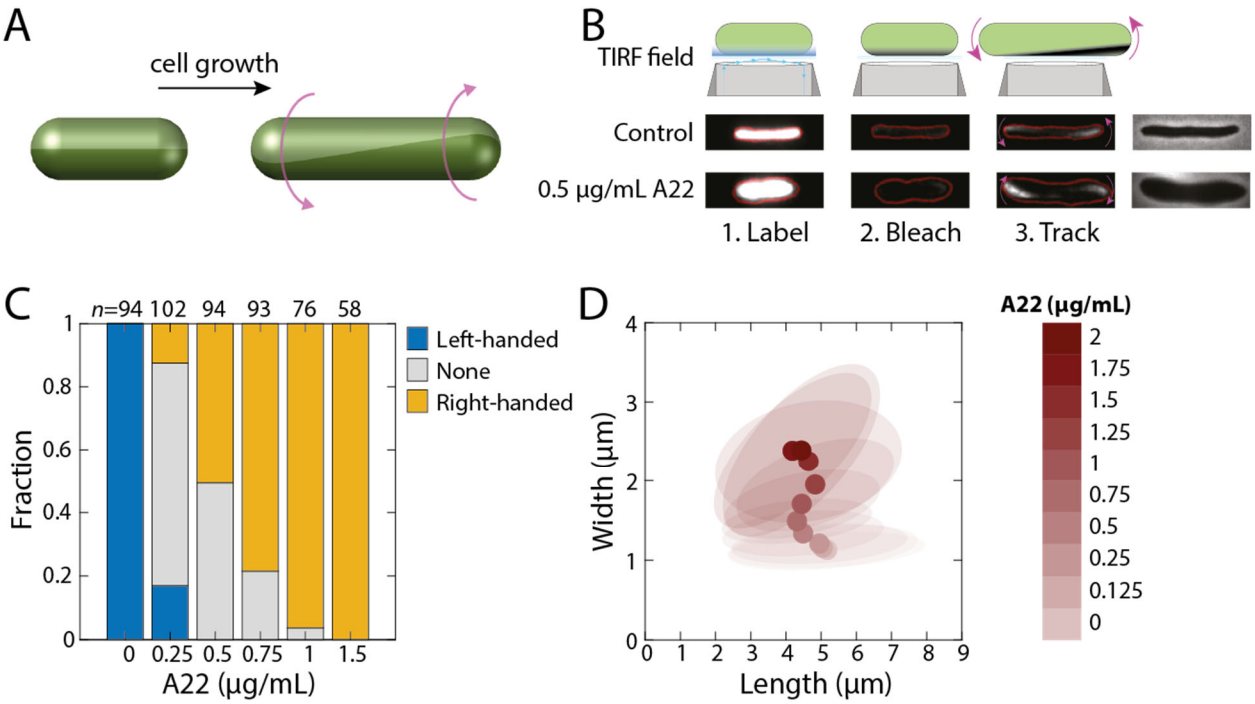

Figure 1: A22 reverses twisting handedness and alters cellular dimensions in *E. coli* DH5α.

A) Schematic of left-handed twisting during elongation of a rod-shaped cell.

B) In the Twist-n-TIRF method, the cell surface is labeled and the side of the cell closest to the cover slip is bleached using a TIRF microscope. During subsequent TIRF imaging at lower intensity, unbleached parts of the cell appear associated with cell twisting (Methods). Rightmost panel: phase-contrast images. A22-treated *E. coli* DH5α cells treated with A22 are typically shorter and wider than untreated cells and twist with opposite handedness during the tracking step; note the appearance of fluorescence on the lower left and upper right in the A22-treated cell, as opposed to the upper left and lower right in the untreated cell.

C) In the absence of A22, virtually all *E. coli* DH5α cells exhibit left-handed twisting, while cells treated with 1.5 μg/mL A22 exhibit right-handed twisting. The number of cells (*n*) is indicated above each bar.

D) *E. coli* DH5α cell width during log-phase growth in liquid increases as a function of A22 concentration. For concentrations <1 μg/mL, cell length decreases with increasing A22 concentration. Circles represent mean dimensions and ellipses represent the covariance matrix of length and width. *n*>50 cells were quantified for each condition.

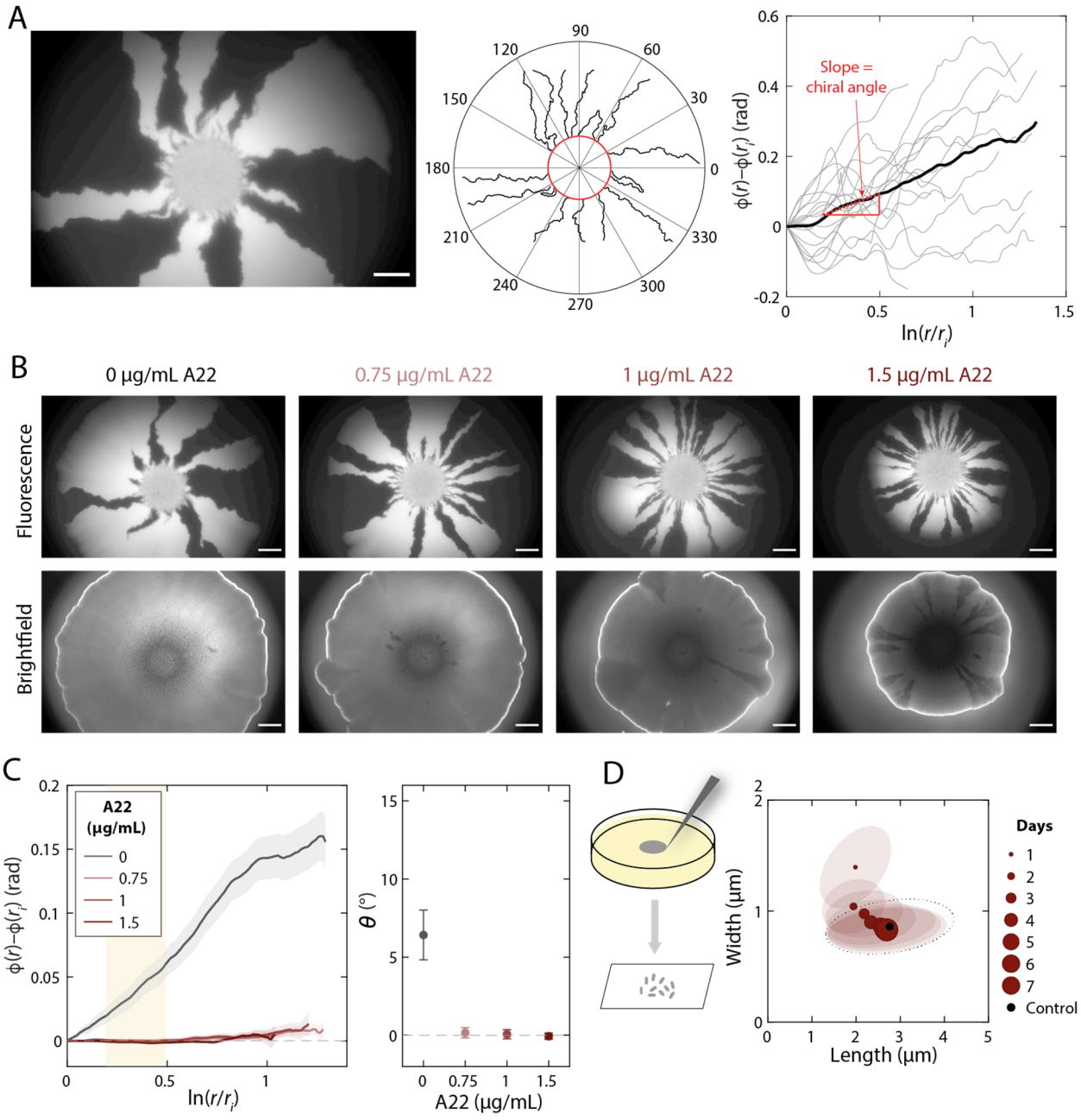

Figure 2: A22 treatment reduces colony chiral angle.

A) Genetic demixing during *E. coli* DH5α colony growth results in monoclonal sectors (left). Although the shape of the boundaries between light (YFP) and dark sectors (middle) appeared stochastic, quantitative image analysis revealed an overall clockwise rotation of sector boundaries when viewed from the top (air interface).

Right: the slope (red) of the mean (thick black curve) is defined as the chiral angle. Scale bar: 1 mm.

B) Images of typical colonies after 7 days of growth on plates with various concentrations of A22 illustrate that colony growth is hindered by A22. The bright outline in the brightfield images denotes the colony border. Sector boundaries were straighter at higher A22 concentrations. Scale bars: 1 mm.

C) Left: mean rotation of sector boundaries at various A22 concentration. Right: the chiral angle decreases at higher A22 concentrations. Each data point is the average of $n \geq 5$ colonies. Error bars represent 1 standard deviation.

D) During colony growth in the presence of 1.5 μg/mL A22, cellular dimensions gradually revert back to those of cells grown in colonies in the absence of A22, suggesting adaptation to A22.

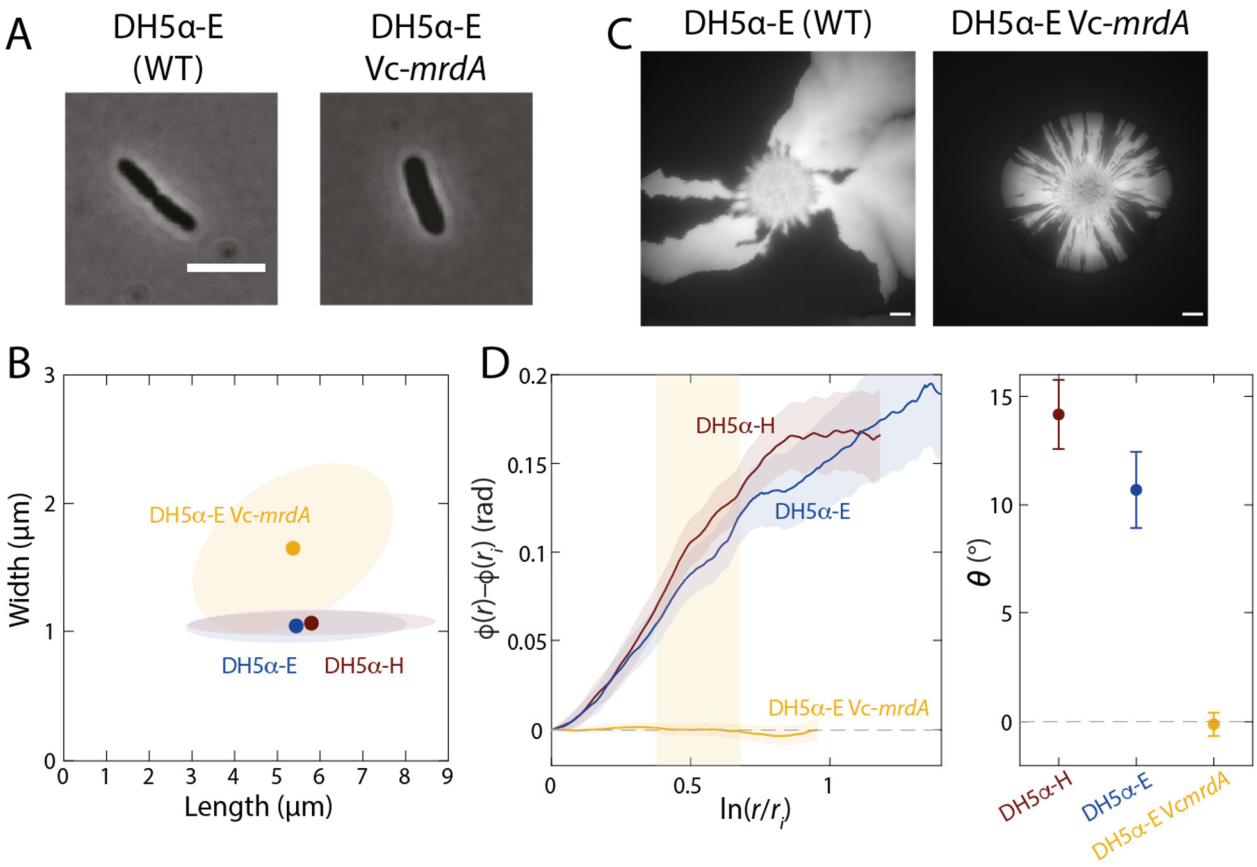

Figure 3: A genetic perturbation that causes cells to become wider eliminates colony chirality.

A,B) Heterologous expression of the *mrdA* gene from *Vibrio cholerae* (Vc-*mrdA*) in the *E. coli* DH5α-E Δ*mrdA* background increases cell width during log phase in liquid growth relative to wild-type DH5α-H or DH5α-E cells. In (B), circles represent mean values and ellipses represent the covariance of width and length. n>50 cells were quantified for each strain. Scale bar: 5 μm.

C,D) Colony chirality is reduced by heterologous expression of Vc-*mrdA*. (C) Image of typical colonies after 7 days of growth. Scale bars: 1 mm. (D) Left: mean rotation of sector boundaries for each strain. Right: the chiral angle is essentially zero for the Vc-

538 *mrdA* strain. Each data point is the average of $n \geq 5$ colonies. Error bars represent 1

539 standard deviation.

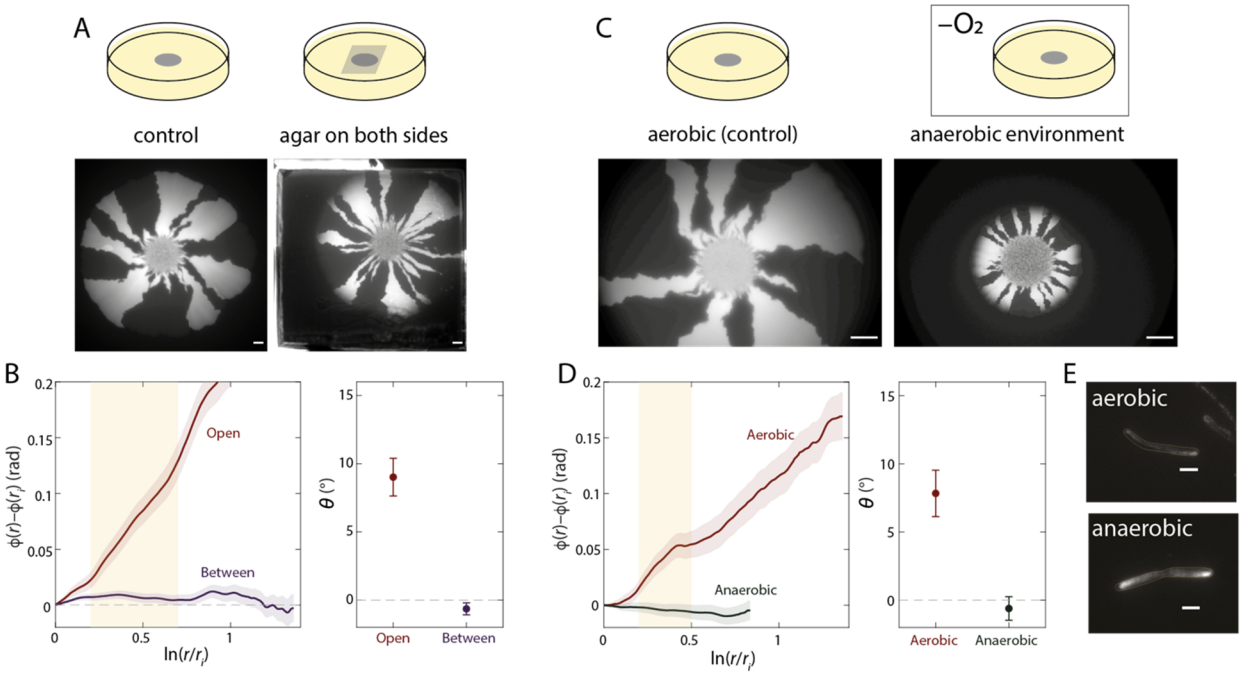

Figure 4: Colony chirality is decreased during growth when sandwiched between agar surfaces or in anaerobic conditions.

A) Top: schematic of control experiments with an air-agar interface ("Open", left) and sandwiched between two agar surfaces ("Between", right) (Methods). Bottom: representative colonies for each condition. Sector boundaries were straighter in the sandwiched colony. Scale bars: 1 mm.

B) Left: mean rotation of sector boundaries in each condition in (A). Right: the chiral angle is essentially zero for sandwiched colonies. Each data point is the average of $n \geq 5$ colonies. Error bars represent 1 standard deviation.

C) Top: schematic of growth in aerobic conditions and in an anaerobic chamber. Bottom: representative colonies for each condition. Sector boundaries were straighter during anaerobic growth. Scale bars: 1 mm.

D) Left: mean rotation of sector boundaries in each condition in (C). Right: the chiral angle is essentially zero during anaerobic growth. Each data point is the average of $n \geq 5$ colonies. Error bars represent 1 standard deviation.

E) DH5α cells still exhibit twisting at the single-cell level during anaerobic growth at 37 °C, as revealed by Twist-n-TIRF. For both aerobic and anaerobic growth, all cells whose handedness could be reliably classified were left-handed (n=43, aerobic; n=31, anaerobic). Scale bars: 2 μm.

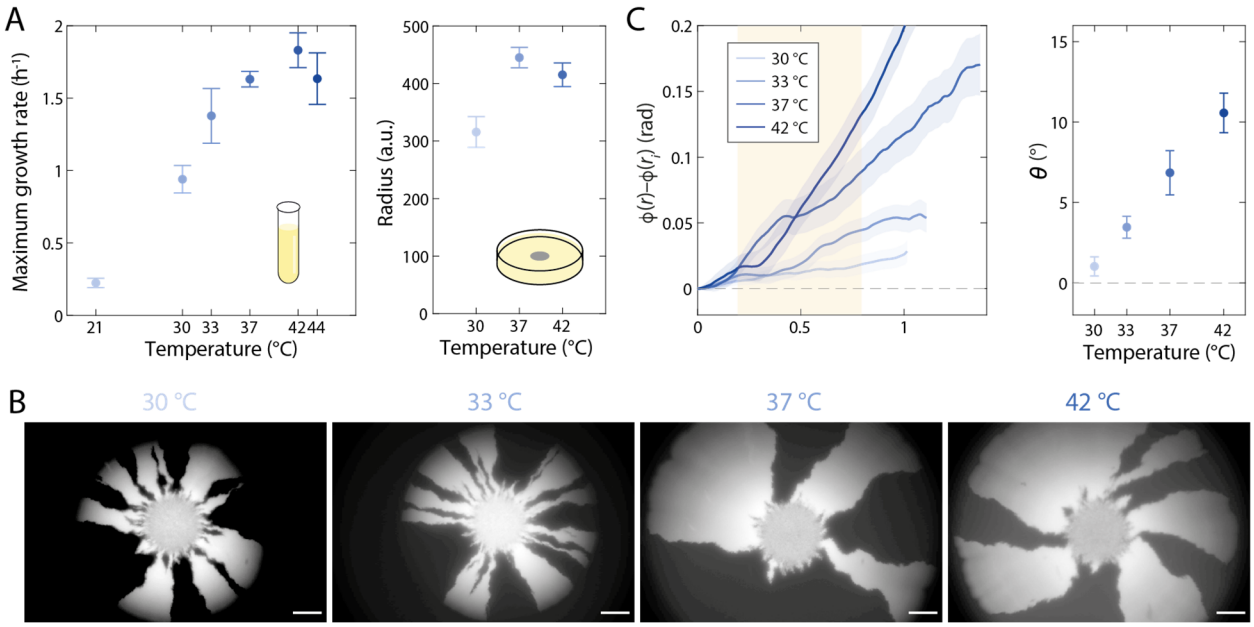

Figure 5: Chiral angle increases with increasing temperature.

A) *E. coli* DH5α Growth depends on temperature. Left: maximum growth rate in liquid peaks at 42 °C. Right: Colony radius is higher at 37 °C than at 30 or 42 °C.

B) Images of representative colonies show increasing chirality at higher temperatures. Scale bars: 1 mm.

C) Left: mean rotation of sector boundaries at each temperature. Right: the chiral angle continues to increase with increasing temperature, even at 42 °C. Each data point is the average of $n \geq 5$ colonies. Error bars represent 1 standard deviation.

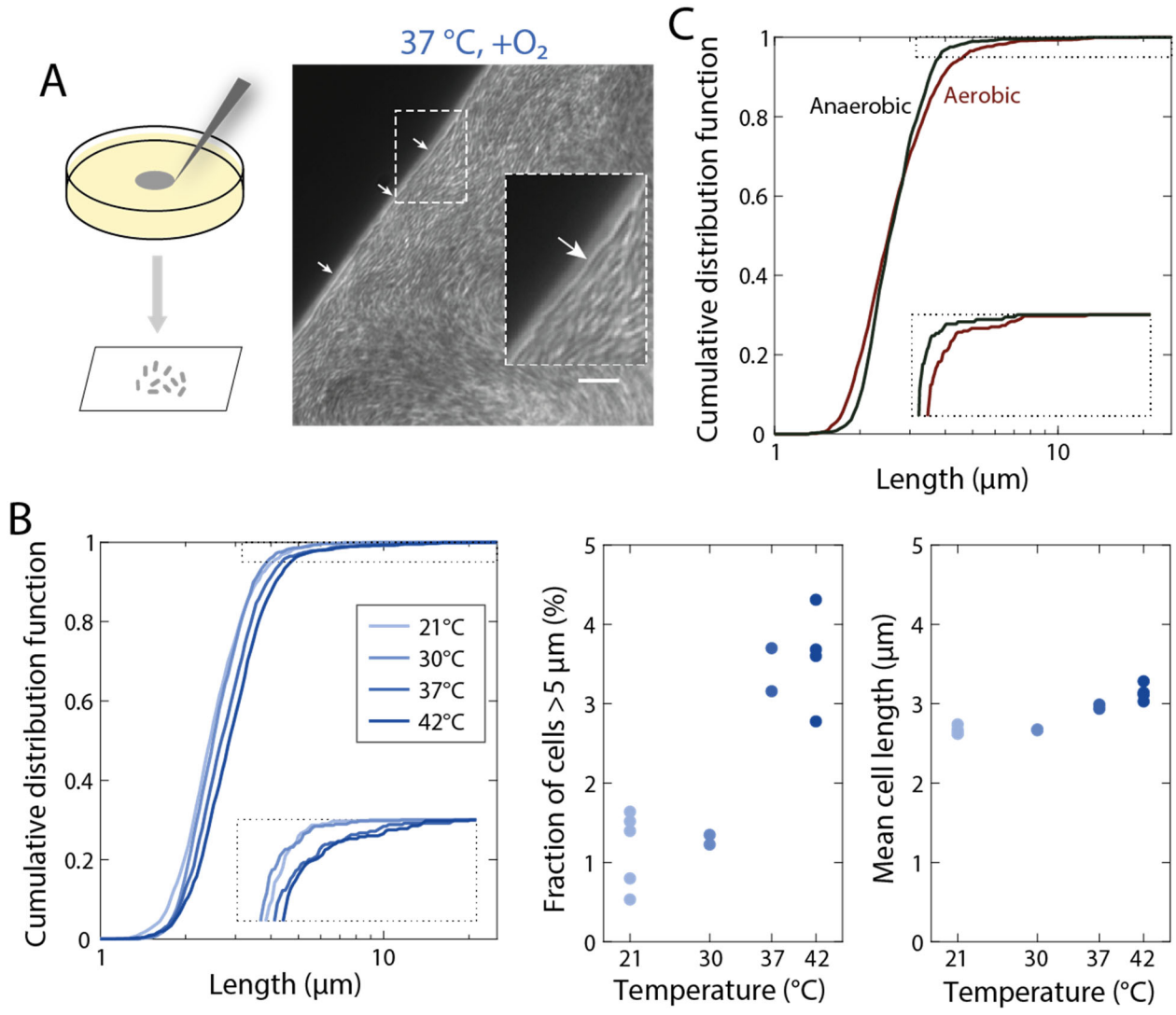

Figure 6: Conditions with enhanced colony chirality exhibit increased fractions of filamentous cells at the colony edge.

A) Left: schematic of sampling from the colony edge. Right: imaging of the colony edge reveals filamentous cells at the border (arrows). Inset is a 200% zoom-in of the region surrounded by the dashed white line highlighting a filamentous cell.

B) At higher temperatures, a larger fraction of the population exhibits filamentation. Left: the cumulative distribution function of cell length shifts to the right at increasing temperature. The inset is a zoom-in of the dotted region. Middle: the fraction of cells

578 with length >5 μm in samples from the edge of colonies increases at increasing
579 temperature. Right: mean cell length also increases slightly with increasing
580 temperature. Each circle was computed from ≥16 fields of view from a sample from a
581 distinct colony.

582 C) During aerobic growth, a larger fraction of the population exhibits filamentation
583 compared with anaerobic growth. The inset is a zoom-in of the dotted region.

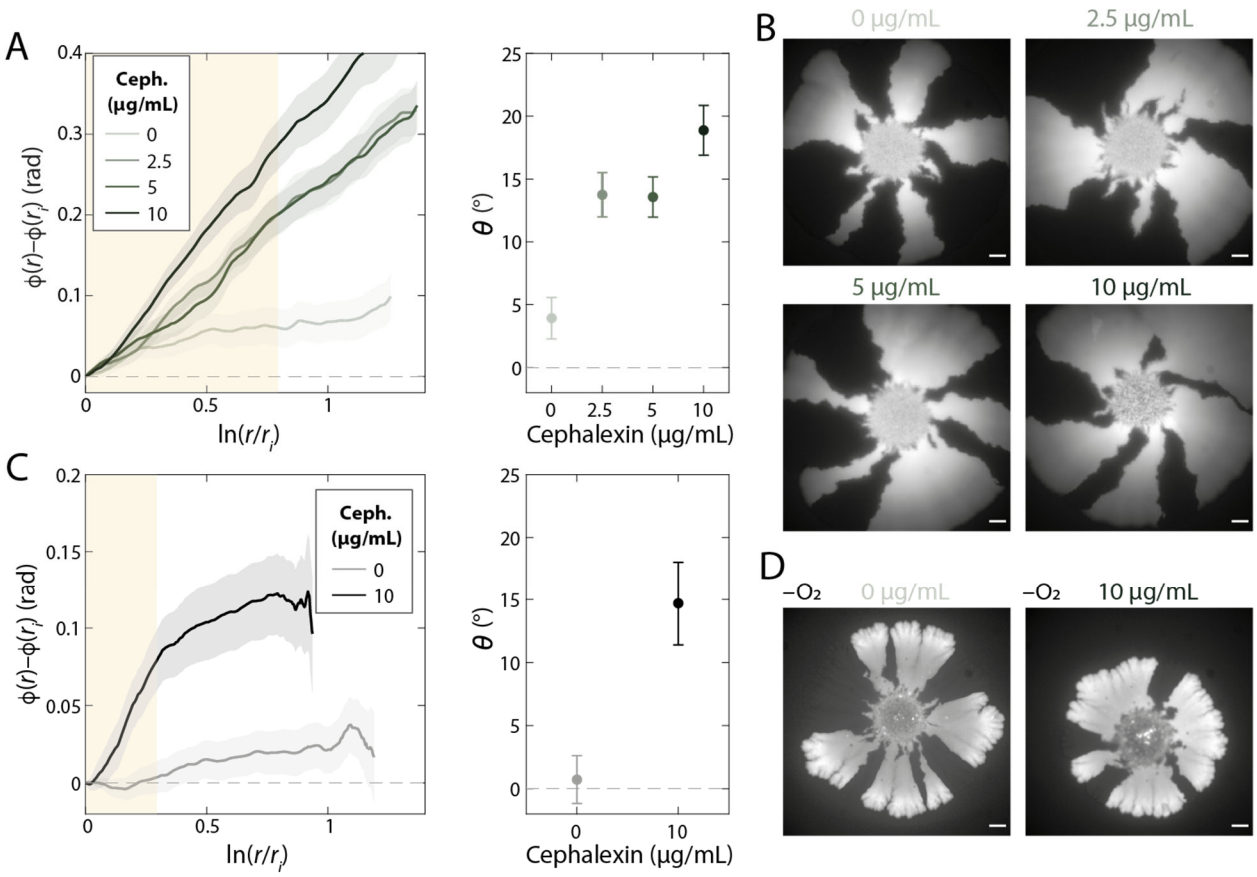

Figure 7: Division inhibition using cephalexin results in enhanced chirality during aerobic growth and the introduction of chirality during anaerobic growth.

A) Left: mean rotation of sector boundaries of aerobically grown DH5α wild-type colonies with various concentrations of cephalexin. Right: the chiral angle increases with increasing cephalexin concentration. Each data point is the average of $n \geq 5$ colonies. Error bars represent 1 standard deviation.

B) Representative colonies grown aerobically with various concentrations of cephalexin. Scale bars: 1 mm.

C) Left: mean rotation of sector boundaries of anaerobically grown DH5α wild-type colonies without and with cephalexin. Right: in the presence, but not in the absence,

595 of cephalexin colonies exhibit chirality. Each data point is the average of $n \geq 5$

596 colonies. Error bars represent 1 standard deviation.

597 D) Representative colonies grown anaerobically without and with 10 μg/mL

598 cephalexin. Scale bars: 1 mm.

599 **References**

600

601 1. P. Satir, Chirality of the cytoskeleton in the origins of cellular asymmetry. *Philos*
602 *Trans R Soc Lond B Biol Sci* **371** (2016).
603 2. H. Shi, D. A. Quint, G. M. Grason, A. Gopinathan, K. C. Huang, Chiral twisting in a
604 bacterial cytoskeletal polymer affects filament size and orientation. *Nat Commun* **11**,
605 1408 (2020).
606 3. S. Hozumi *et al.*, An unconventional myosin in Drosophila reverses the default
607 handedness in visceral organs. *Nature* **440**, 798-802 (2006).
608 4. M. Inaki, J. Liu, K. Matsuno, Cell chirality: its origin and roles in left-right asymmetric
609 development. *Philos Trans R Soc Lond B Biol Sci* **371** (2016).
610 5. S. R. Naganathan, S. Furthauer, M. Nishikawa, F. Julicher, S. W. Grill, Active torque
611 generation by the actomyosin cell cortex drives left-right symmetry breaking. *Elife*
612 **3**, e04165 (2014).
613 6. T. Shoji *et al.*, Plant-specific microtubule-associated protein SPIRAL2 is required for
614 anisotropic growth in Arabidopsis. *Plant Physiol* **136**, 3933-3944 (2004).
615 7. T. S. Ursell *et al.*, Rod-like bacterial shape is maintained by feedback between cell
616 curvature and cytoskeletal localization. *Proceedings of the National Academy of*
617 *Sciences of the United States of America* **111**, E1025-1034 (2014).
618 8. S. Wang, L. Furchtgott, K. C. Huang, J. W. Shaevitz, Helical insertion of peptidoglycan
619 produces chiral ordering of the bacterial cell wall. *Proceedings of the National*
620 *Academy of Sciences of the United States of America* **109**, E595-604 (2012).

621 9. N. H. Mendelson, Helical growth of Bacillus subtilis: a new model of cell growth.
622 *Proceedings of the National Academy of Sciences of the United States of America* **73**,
623 1740-1744 (1976).
624 10. J. V. Holtje, Growth of the stress-bearing and shape-maintaining murein sacculus of
625 Escherichia coli. *Microbiol Mol Biol Rev* **62**, 181-203 (1998).
626 11. K. D. Young, The selective value of bacterial shape. *Microbiol Mol Biol Rev* **70**, 660-
627 703 (2006).
628 12. L. Furchtgott, N. S. Wingreen, K. C. Huang, Mechanisms for maintaining cell shape in
629 rod-shaped Gram-negative bacteria. *Mol Microbiol* **81**, 340-353 (2011).
630 13. Z. Gitai, N. Dye, L. Shapiro, An actin-like gene can determine cell polarity in bacteria.
631 *Proceedings of the National Academy of Sciences of the United States of America* **101**,
632 8643-8648 (2004).
633 14. Z. Gitai, N. A. Dye, A. Reisenauer, M. Wachi, L. Shapiro, MreB actin-mediated
634 segregation of a specific region of a bacterial chromosome. *Cell* **120**, 329-341
635 (2005).
636 15. C. Tropini *et al.*, Principles of bacterial cell-size determination revealed by cell-wall
637 synthesis perturbations. *Cell Rep* **9**, 1520-1527 (2014).
638 16. S. van Teeffelen *et al.*, The bacterial actin MreB rotates, and rotation depends on cell-
639 wall assembly. *Proceedings of the National Academy of Sciences of the United States of*
640 *America* **108**, 15822-15827 (2011).
641 17. O. Hallatschek, P. Hersen, S. Ramanathan, D. R. Nelson, Genetic drift at expanding
642 frontiers promotes gene segregation. *Proceedings of the National Academy of*
643 *Sciences of the United States of America* **104**, 19926-19930 (2007).

644 18. O. Hallatschek, D. R. Nelson, Gene surfing in expanding populations. *Theor Popul Biol*
645 **73**, 158-170 (2008).
646 19. K. S. Korolev, J. B. Xavier, D. R. Nelson, K. R. Foster, A quantitative test of population
647 genetics using spatiogenetic patterns in bacterial colonies. *Am Nat* **178**, 538-552
648 (2011).
649 20. L. Jauffred, R. Munk Vejborg, K. S. Korolev, S. Brown, L. B. Oddershede, Chirality in
650 microbial biofilms is mediated by close interactions between the cell surface and the
651 substratum. *ISME J* **11**, 1688-1701 (2017).
652 21. M. Silvis *et al.*, Morphological and transcriptional responses to essential-gene
653 depletion in *Escherichia coli*. (2021).
654 22. B. G. Spratt, Distinct penicillin binding proteins involved in the division, elongation,
655 and shape of Escherichia coli K12. *Proceedings of the National Academy of Sciences*
656 **72**, 2999-3003 (1975).
657 23. S. J. Remington, Fluorescent proteins: maturation, photochemistry and
658 photophysics. *Curr Opin Struct Biol* **16**, 714-721 (2006).
659 24. R. Y. Tsien, The green fluorescent protein. *Annu Rev Biochem* **67**, 509-544 (1998).
660 25. M. A. Barber, The Rate of Multiplication of Bacillus Coli at Different Temperatures.
661 *The Journal of Infectious Diseases* **5**, 379-400 (1908).
662 26. M. Schaechter, O. Maaløe, N. Kjeldgaard, Dependency on medium and temperature of
663 cell size and chemical composition during balanced grown of Salmonella
664 typhimurium. *J. Gen. Microbiol.* **19**, 592-606 (1958).

665 27. P. J. Hedge, B. G. Spratt, Amino acid substitutions that reduce the affinity of
666 penicillin-binding protein 3 of Escherichia coli for cephalexin. *Eur J Biochem* **151**,
667 111-121 (1985).
668 28. M. R. Warren *et al.*, Spatiotemporal establishment of dense bacterial colonies
669 growing on hard agar. *Elife* **8** (2019).
670 29. W. P. Smith *et al.*, Cell morphology drives spatial patterning in microbial
671 communities. *Proceedings of the National Academy of Sciences of the United States of*
672 *America* **114**, E280-E286 (2017).
673 30. J. van Gestel, F. J. Weissing, O. P. Kuipers, A. T. Kovacs, Density of founder cells affects
674 spatial pattern formation and cooperation in Bacillus subtilis biofilms. *ISME J* **8**,
675 2069-2079 (2014).
676 31. E. Ben-Jacob, I. Cohen, H. Levine, Cooperative self-organization of microorganisms.
677 *Advances in Physics* **49**, 395-554 (2000).
678 32. J. C. Tsai, F. Ye, J. Rodriguez, J. P. Gollub, T. C. Lubensky, A Chiral Granular Gas. *Phys.*
679 *Rev. Lett.* **94**, 214301 (2005).
680 33. S. Fürthauer, M. Strempel, S. W. Grill, F. Jülicher, Active chiral fluids. *Eur. Phys. J. E*
681 **35**, 89 (2012).
682 34. K. Drescher *et al.*, Dancing Volvox : Hydrodynamic Bound States of
683 Swimming Algae. *Phys. Rev. Lett.* **102**, 168101 (2009).
684 35. A. P. Petroff, X.-L. Wu, A. Libchaber, Fast-Moving Bacteria Self-Organize into Active
685 Two-Dimensional Crystals of Rotating Cells. *Phys. Rev. Lett.* **114**, 158102 (2015).
686 36. J. Yan, S. C. Bae, S. Granick, Rotating crystals of magnetic Janus colloids. *Soft Matter*
687 **11**, 147-153 (2015).

688 37. A. Snezhko, Complex collective dynamics of active torque-driven colloids at
689 interfaces. *Current Opinion in Colloid & Interface Science* **21**, 65-75 (2016).
690 38. B. C. van Zuiden, J. Paulose, W. T. M. Irvine, D. Bartolo, V. Vitelli, Spatiotemporal
691 order and emergent edge currents in active spinner materials. *Proceedings of the*
692 *National Academy of Sciences* **113**, 12919-12924 (2016).
693 39. N. H. P. Nguyen, D. Klotsa, M. Engel, S. C. Glotzer, Emergent Collective Phenomena in
694 a Mixture of Hard Shapes through Active Rotation. *Phys. Rev. Lett.* **112**, 075701
695 (2014).
696 40. K. Yeo, E. Lushi, P. M. Vlahovska, Collective Dynamics in a Binary Mixture of
697 Hydrodynamically Coupled Microrotors. *Phys. Rev. Lett.* **114**, 188301 (2015).
698 41. C. del Junco, L. Tociu, S. Vaikuntanathan, Energy dissipation and fluctuations in a
699 driven liquid. *Proceedings of the National Academy of Sciences* **115**, 3569-3574
700 (2018).
701 42. C. Scholz, M. Engel, T. Pöschel, Rotating robots move collectively and self-organize.
702 *Nature Communications* **9**, 931 (2018).
703 43. A. Souslov, K. Dasbiswas, M. Fruchart, S. Vaikuntanathan, V. Vitelli, Topological
704 Waves in Fluids with Odd Viscosity. *Phys. Rev. Lett.* **122**, 128001 (2019).
705 44. G. Baardink, G. Cassella, L. Neville, P. A. Milewski, A. Souslov, Complete absorption of
706 topologically protected waves. *arXiv:2010.07342 [cond-mat, physics:physics]* (2020).
707 45. D. Banerjee, A. Souslov, A. G. Abanov, V. Vitelli, Odd viscosity in chiral active fluids.
708 *Nature Communications* **8**, 1573 (2017).
709 46. A. Souslov, A. Gromov, V. Vitelli, Anisotropic odd viscosity via a time-modulated
710 drive. *Phys. Rev. E* **101**, 052606 (2020).

711 47. V. Soni *et al.*, The odd free surface flows of a colloidal chiral fluid. *Nat. Phys.* **15**,
712 1188-1194 (2019).
713 48. B. G. A, K. S. Korolev, Chirality provides a direct fitness advantage and facilitates
714 intermixing in cellular aggregates. *PLoS Comput Biol* **14**, e1006645 (2018).
715 49. N. Stuurman, N. Amdodaj, R. Vale, μManager: open source software for light
716 microscope imaging. *Microscopy Today* **15**, 42-43 (2007).
717 50. T. Ursell *et al.*, Rapid, precise quantification of bacterial cellular dimensions across a
718 genomic-scale knockout library. *BMC Biol* **15**, 17 (2017).
719 51. O. Sliusarenko, J. Heinritz, T. Emonet, C. Jacobs-Wagner, High-throughput, subpixel
720 precision analysis of bacterial morphogenesis and intracellular spatio-temporal
721 dynamics. *Molecular microbiology* **80**, 612-627 (2011).
722 52. D. A. Van Valen *et al.*, Deep Learning Automates the Quantitative Analysis of
723 Individual Cells in Live-Cell Imaging Experiments. *PLoS Comput Biol* **12**, e1005177
724 (2016).

725